European Polymer Journal 186 (2023) 111830

Contents lists available at ScienceDirect

European Polymer Journal

journal homepage: www.elsevier.com/locate/europolj

Fluorine and hydroxyl containing unsymmetrical *a*-diimine Ni (II) dichlorides with improved catalytic performance for ethylene polymerization

Ruikai Wu [a,b], Lucas Stieglitz [c], Sandro Lehner [a], Milijana Jovic [a], Daniel Rentsch [d], Antonia Neels [e], Sabyasachi Gaan [a,*], Bernhard Rieger [c], Manfred Heuberger [a,b,*]

[a] Laboratory of Advanced Fibers, Empa, Swiss Federal Laboratories for Materials Science and Technology, Lerchenfeldstrasse 5, 9014 St. Gallen, Switzerland
[b] Department of Materials, ETH Zurich, 8092 Zurich, Switzerland
[c] WACKER-Chair of Macromolecular Chemistry, Catalysis Research Center, Technical University Munich, Lichtenbergstraße 4, 85748 Garching, Germany
[d] Laboratory for Functional Polymers, Empa, Swiss Federal Laboratories for Materials Science and Technology, Überlandstrasse 129, 8600 Dübendorf, Switzerland
[e] Center for X-ray Analytics, Empa, Swiss Federal Laboratories for Materials Science and Technology, Überlandstrasse 129, 8600 Dübendorf, Switzerland

ARTICLE INFO

Keywords:
a-Diimine Ni (II) complexes
Ethylene polymerization
Catalytic behavior
Polyethylene, polymer branches
High molecular weight

ABSTRACT

A series of new tailored *a*-diimine Ni (II) complexes (**Ni-OH**, **Ni-FOH**, **Ni-PhOH,** and **Ni-PhFOH**) containing bulky *ortho-N*-aryl groups with various dibenzhydryl substitutes was successfully synthesized, characterized and applied in ethylene polymerization. The *a*-diimine ligands and Ni (II) complexes were characterized by ^{1}H, ^{19}F, and ^{13}C NMR, elemental analysis, and high resolution electrospray ionization mass spectrometry (ESI-HRMS). The X-ray crystallographic study of metal complexes **Ni-OH**, **Ni-FOH**, and **Ni-PhFOH** revealed their distorted tetrahedral geometry. An unsymmetrical steric-enhancement design approach was employed to modulate the competition between the monomer insertion and the chain-walking process in ethylene polymerization. This facile design resulted in a high catalytic activity and yielded high molecular weight PE. The catalytic activity of these complexes was optimized by varying the polymerization conditions (temperature, time, and ethylene pressure), use of co-catalysts and variation of the Al/Ni ratio. When activated with modified methylaluminoxane (MMAO), these Ni complexes exhibited the activity as high as 29.1 $\times$ 10^6 g of PE (mol of Ni)$^{-1}$ h^{-1}), with a molecular weight of 1.81 $\times$ 10^6 g mol^{-1}. Their thermal stability was well pronounced at elevated temperatures; high activity of 2.88 $\times$ 10^6 g of PE (mol of Ni)$^{-1}$ h^{-1} and high molecular weight PE (0.86 $\times$ 10^6 g mol^{-1}obtained at 90 °C). PEs with tunable branches and high melting points (127.5 °C) were obtained, which is a typical feature of LLDPE. The incorporation of fluorine atoms on *N*-aryl groups had a strong positive influence on the catalytic activity of the Ni complexes and favored the chain-growth process in the ethylene polymerization. Surprisingly, the simultaneous presence of terminal hydroxyl group in these complexes did not adversely affect their catalytic activity, while offering the possibility for covalent attachment to the solid supports for future heterogeneous polymerization.

1. Introduction

PE-based polymers represent one of the most important materials class in our daily life due to their superb mechanical properties, chemical stability and low production costs [1]. In this field, the coordination-insertion polymerization via transition-metal complexes plays a crucial role in synthesis of polyethylene materials. Compared to the early-transition metal complexes, the late-transition metal-based analogues exhibit superior performance in such catalyzed polymerization [2–4]. These complexes are tolerant to moisture and air, enabling a long-term storage and delivery without inert atmosphere protection. Furthermore, due to the low oxophilicity, they are even able to perform the ethylene copolymerization with polar monomers, yielding PE copolymers containing polar groups [5–8]. Compared to the conventional multi-site heterogeneous catalysts, the single-site catalytic metal allows for the production of PE with narrow molecular weight distributions (PDI). The

* Corresponding authors at: Laboratory of Advanced Fibers, Empa, Swiss Federal Laboratories for Materials Science and Technology, Lerchenfeldstrasse 5, 9014 St. Gallen, Switzerland (M.H.).
E-mail addresses: Sabyasachi.Gaan@empa.ch (S. Gaan), Manfred.Heuberger@empa.ch (M. Heuberger).

https://doi.org/10.1016/j.eurpolymj.2023.111830
Received 29 November 2022; Received in revised form 3 January 2023; Accepted 9 January 2023
Available online 13 January 2023

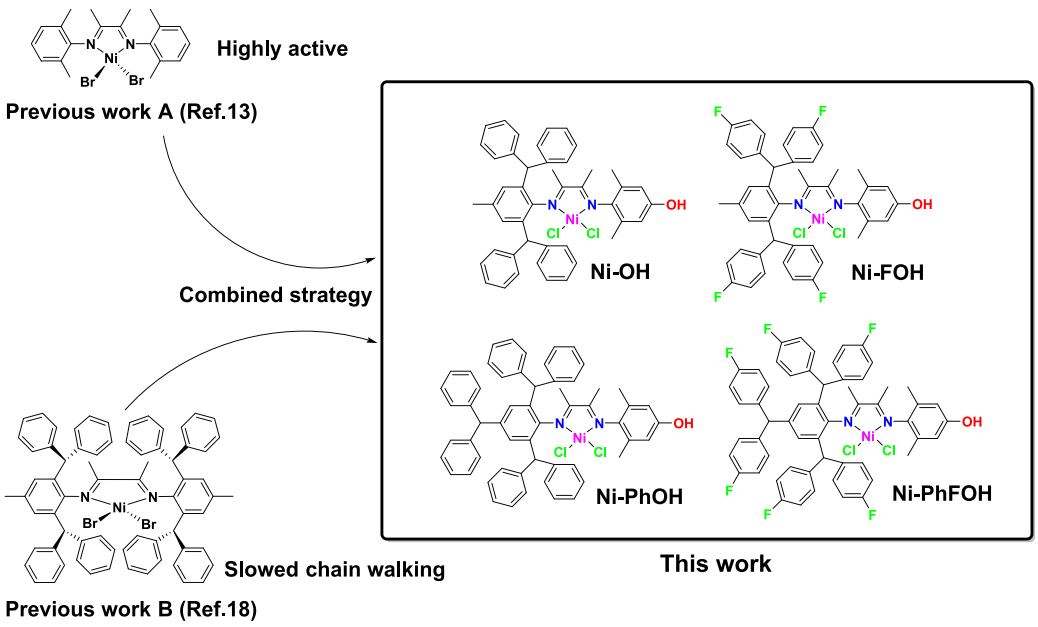

Fig. 1. Previous studies on *α*-diimine Ni (II) complexes and design strategy of this work.

polymeric microstructures can be modulated *via* a modification of the complexes structures, leading to a variation in the molecular weight (M_w), PDI, melting transition, density, crystallinity, and branching density. The macroscopic characteristics such as mechanics, surface wettability, chemical and thermal stability, optics, and viscosity of PE can indirectly be altered by suitable modifications of the complex structures [9,10]. Thus, late-transition metal-catalyzed polymerization can be considered as one of the most promising approaches for future industrial olefin polymerization [2,10–13].

The *α*-diimine Ni/Pd complexes are one of the best-studied and long-examined late-transition metal-based catalysts for ethylene polymerization. The initial work (**A** in Fig. 1) of *Brookhart et al.* demonstrated the high activity (10^7 g of PE (mol of Ni)$^{-1}$ h^{-1}) and great potential of such catalysts [14,15]. One of the major advantages of these complexes is the ability to produce thermoplastic-elastomers (TPEs) like branched PE *via* chain-walking mechanism, by use of ethylene as the only reactive monomer [16–18]. The chain walking process involves a competition between the chain growth and chain walking during the monomer insertion process. Cationic alkyl-metal active species migrate along the polyethylene backbone *via* rapid *β*-H elimination and reinsertion, leading to the formation of branched structures [19,20]. As reported previously, the remote substitutions, *N*-aryl groups and backbones are considered as the main factors that control the catalytic behavior of the *α*-diimine metal complexes. For example, the steric accumulation on the *N*-aryl group (*e.g.* **B** in Fig. 1) significantly changes the catalytic performance of the Ni center [21–23]. These bulky substituents (especially in *ortho* position of the *N*-aryl) act as a shield and offer confined space for monomer insertion, which slows down both the chain-transfer and the chain-walking process. A limited coordination space around the metal center favors a chain-growth mechanism, leading to a more linear and high molecular weight PE [21,24–31]. Additionally, electron-withdrawing groups could considerably enhance the catalytic performance of the cationic alkyl-metal center – the fluorine effect is of great importance in the application of the olefin polymerization, as the fluorine atom has an electron-withdrawing character due to its inductive effects [32–35]. In contrast to saturated electron-withdrawing groups, the fluorine exhibits π interactions with the aromatic rings. The interaction between the catalytic metal centers with fluorine atoms has been described in previous work, where it was shown to have great influences on the catalytic behavior in polymerization process [26,36–39]. The side-arm (i.e. steric and electronic) effects of the ligand moiety create distinctive coordination environments around the catalytic metal center, leading to important variety of polymer properties [2,7,40–44].

Currently, numerous studies related to the synthesis of the new *α*-diimine Ni (II) complexes have been reported, where the symmetric arrangement of bulky *N*-aryls has been the focus [20,45]. However, the catalytic activity is decreased by the limited monomer access into the confined coordination space of the active metal center. The ligands containing bulky groups on both *N*-aryls tend to exhibit lower (1 or 2 order of magnitudes) catalytic activity than **A** in Fig. 1 [21,46]. As reported previously, it is difficult to simultaneously achieve both the high catalytic activity and high molecular weights. The unsymmetrical *α*-diimine Ni complexes bearing different anilines have been reported since the initial study of benzhydryl-substituted ligands [47,48]. The dibenzhydryl substitutions as the steric groups were incorporated on the first *N*-aryl, while the second *N*-aryl moiety was maintained as the less bulky (methyl group) substituent. The catalytic properties of such unsymmetrical *α*-diimine Ni complexes can be modified by the structural tunes of the solo *N*-aryl substitution with typical electronic and steric features [20,30,48,49].

In this work, a simplified synthetic methodology was followed to synthesize a series of new unsymmetrical *α*-diimine Ni complexes (**Ni-OH**, **Ni-FOH**, **Ni-PhOH** and **Ni-PhFOH** in Fig. 1). The aim of our catalyst design was to realize the typical modulation of ethylene monomer insertion and chain-walking process while still maintaining high activity during the ethylene polymerization. It can be considered as a balancing combination of high activity and suppressed *β*-H elimination. Different steric enhancements (dibenzhydryl substitutions) on the *para/ortho-N*-aryls offer various environments to the coordination-insertion process. In order to systematically check the fluorine effect on the catalytic performance during the ethylene polymerization, the fluorine moiety on the *N*-aryls was synthesized and incorporated on these Ni complexes. The Cl atoms are selected as the affiliation of metal center rather than Br, leading to the formation of the *α*-diimine Ni dichlorides. The various polymerization conditions were optimized in detail, including co-catalyst, Al/Ni ratio, polymerization temperature, lifetime, and ethylene pressure. This facile strategy is expected to realize the further modifications of the catalytic behaviors of the proposed *α*-diimine Ni complexes and polymeric microstructure, such as the branches, M_w, PDI and melting transitions. Additionally, the design of ligands involved the incorporation of hydroxyl group, which could then be used to tether the Ni complexes to solid surfaces for gas- and slurry-phase polymerization.

Although the hydroxyl group is very electron donating and active to the activated metal center, no reduction in the catalytic performance of the *a*-diimine Ni complexes was observed.

2. Experimental

2.1. General considerations

The synthesis of the *a*-diimine ligands and Ni (II) complexes was carried out under air. Contrary to this, ethylene polymerizations were performed under *Schlenk* techniques and inert argon atmosphere protection. All the solvents and starting materials were purchased from Sigma-Aldrich and Chemie-Brunschwig. The ^{1}H, ^{13}C and ^{19}F NMR spectrum of *a*-diimine ligands and Ni complexes were recorded on the Bruker Avance III 400 NMR spectrometer. Elemental analysis was carried out using Elementar-UNICUBE analyzer. M_w and PDI, branching density were determined by a 1260 infinity ii HT-GPC at 160 °C with 1,2,4-trichlorobenzene as the solvent against PS standards. The ESI-HRMS results were analyzed by an UHR-TOF BRUCKER Doltonik (Bremen, Germany) maXis with an ESI-quadrupole time-of flight (qToF) mass spectrometer. The melting points were determined by the differential scanning calorimeter (DSC, 214-Polyma) with second-heating-scan curves. ^{1}H and ^{13}C NMR spectra of the polyethylene were measured by using an ARX-300 spectrometer at 140 °C in bromobenzene- d_6.

2.2. Synthesis and characterization of a-diimine ligands

L-OH

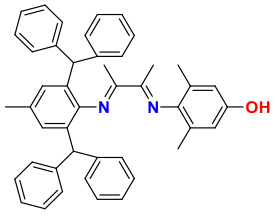

A solution of 3-((2,6-dibenzhydryl-4-methylphenyl)imino)butan-2-one (1.01 g, 2.0 mmol) and 4-amino-3,5-dimethylphenol (0.33 g, 2.4 mmol) in toluene (50 mL) with a catalytic amount of *para*-toluenesulfonic acid (0.035 g, 0.2 mmol) was stirred under refluxed over 36 h. Afterwards, the mixture was cooled down to the room temperature and concentrated under reduced pressure by rotary evaporator. The rest solid was purified by silica column chromatography (Heptane 3/1 Ethyl acetate) to afford **L-OH** as yellow crystalline solid (0.38 g, 30.0 %). ^{1}H NMR (400.2 MHz, DMSO-d_6): δ(ppm) 0.67 (s, 3H), 1.78 (s, 3H), 1.86 (s, 6H), 2.11 (s, 3H), 5.18(s, 2H), 6.49 (s, 2H), 6.61 (s, 2H), 7.00 (d, 4H, J = 8 Hz), 7.07 (d, 4H, J = 8 Hz), 7.17–7.30 (m, 12H), 8.86 (s, 1H). ^{13}C NMR (100.6 MHz, DMSO-d_6): δ(ppm) 13.9, 15.4, 15.5, 17.6, 21.0, 22.1, 28.3, 31.2, 51.7, 114.4, 125.0, 126.2, 126.2, 128.0, 128.2, 128.5, 129.0, 129.3, 130.9, 131.1, 140.2, 142.1, 143.1, 145.2, 152.8, 167.6, 169.6. Anal. Calcd for $C_{45}H_{42}N_2O$ (626.84): C, 86.22; H, 6.75; N, 4.47. Found: C, 86.22; H, 7.01 N, 4.17.

L-FOH

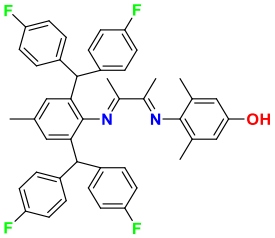

Based on the similar procedure described for **L-OH**, **L-FOH** was synthesized via the reaction of 3-((2,6-bis(bis(4-fluorophenyl)methyl)-4-methylphenyl)imino)butan-2-one (3.48 g, 6 mmol) and 4-amino-3,5-dimethylphenol (1.28 g, 6 mmol) with a catalytic amount of *para*-toluenesulfonic acid (0.105 g, 0.6 mmol) in toluene. **L-FOH** was isolated as yellow crystalline solid (1.85 g, 39.8 %). ^{1}H NMR (400.2 MHz, DMSO-d_6): ^{1}H NMR (400.2 MHz, DMSO-d_6): δ(ppm) 0.84 (s, 3H), 1.76 (s, 3H), 1.85 (s, 6H), 2.13 (s, 3H), 5.21(s, 2H), 6.49 (s, 2H), 6.58 (s, 2H), 6.97–7.13 (m, 16H), 8.86 (s, 1H).^{13}C NMR (100.6 MHz, DMSO- d_6): δ(ppm) 15.5, 15.7, 17.7, 21.0, 50.0, 54.9, 114.4, 114.9, 115.1, 115.2, 115.4, 125.1, 128.0, 130.7, 130.8, 131.0, 131.1, 131.4, 138.2, 138.3, 139.0, 139.1, 140.1, 152.9, 159.4, 159.5, 161.8, 161.9, 167.5, 169.4. ^{19}F NMR (376.5 MHz, DMSO- d_6): δ(ppm) −116.7, −116.4. Anal. Calcd for $C_{45}H_{38}F_4N_2O$ (698.81): C, 77.35; H, 5.48; N, 4.01. Found: C, 77.23; H, 5.56; N, 3.63.

L-PhOH

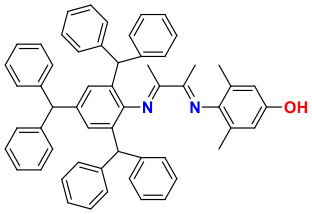

Based on the similar procedure described for **L-OH**, **L-PhOH** was synthesized via the reaction of 3-((2,4,6-tribenzhydrylphenyl)imino) butan-2-one (3.33 g, 5 mmol) and 4-amino-3,5-dimethylphenol (0.69 g, 5 mmol) with a catalytic amount of *para*-toluenesulfonic acid (0.087 g, 0.5 mmol) in toluene. **L-PhOH** was isolated as yellow crystalline solid (1.21 g, 31.0 %). ^{1}H NMR (400.2 MHz, DMSO- d_6): δ(ppm) 0.72 (s, 3H), 1.77 (s, 3H), 1.85 (s, 6H), 5.16 (s, 2H), 5.39 (s, 1H), 6.49 (s, 2H), 6.60 (s, 2H), 6.87–6.97 (m, 12H), 7.11–7.23 (m, 18H) 8.85 (s, 1H). ^{13}C NMR (100.6 MHz, DMSO- d_6): δ(ppm) 16.0, 16.1, 18.1, 52.2, 55.6, 114.8, 125.4, 126.4, 126.5, 126.7, 128.5, 128.6, 128.9, 129.0, 129.2, 129.2, 129.6, 131.4, 137.7, 140.7, 142.5, 143.4, 144.6, 146.1, 153.4, 168.1, 170.1. Anal. Calcd for $C_{57}H_{50}N_2O$ (779.04): C, 87.88; H, 6.47; N, 3.60. Found: C, 88.04; H, 6.48; N, 3.68.

L-PhFOH

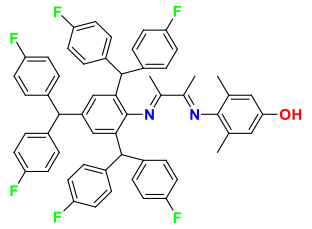

Based on the similar procedure described for **L-OH**, **L-PhFOH** was synthesized via the reaction of 3-((2,4,6-tris(bis(4-fluorophenyl)methyl) phenyl)imino)butan-2-one (1.54 g, 2 mmol) and 4-amino-3,5-dimethylphenol (0.28 g, 2 mmol) with a catalytic amount of *para*-toluenesulfonic acid (0.035 g, 0.2 mmol) in toluene. **L-PhFOH** was isolated as yellow crystalline solid (0.79 g, 44.7 %). ^{1}H NMR (400.2 MHz, DMSO- d_6): δ(ppm) 0.90 (s, 3H), 1.71 (s, 3H), 1.84 (s, 6H), 5.19 (s, 2H), 5.49 (s, 1H), 6.37 (s, 2H), 6.49 (s, 2H), 6.87–6.90 (m, 4H), 6.95–7.08 (m, 18H) 8.86 (s, 1H). ^{13}C NMR (100.6 MHz, DMSO- d_6): δ(ppm) 14.4, 15.7, 16.4, 18.1, 22.5, 28.8, 31.7, 50.5, 53.5, 114.8, 115.2, 115.3, 115.5, 115.5, 115.6, 115.8, 125.5, 128.9, 130.8, 130.9, 130.9, 131.0, 131.2, 131.3, 131.4, 137.9, 138.5, 138.5, 139.2, 139.2, 140.4, 140.4, 140.5, 146.0, 153.4, 159.9, 159.9, 162.3, 162.4, 167.9, 169.7. ^{19}F NMR (376.5 MHz, DMSO-d_6): δ(ppm) −116.8, −116.3. Anal. Calcd for $C_{57}H_{44}F_6N_2O$ (886.98): C, 77.19; H, 5.00; N, 3.16. Found: C, 77.39; H, 5.14; N, 3.09.

2.3. Synthesis and characterization of a-diimine Ni complexes

Ni-OH

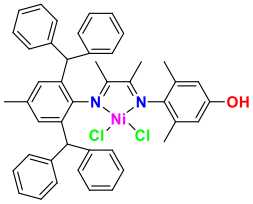

$NiCl_2{\cdot}6H_2O$ (0.209 g 0.88 mmol) and **L-OH** (0.55 g, 0.88 mmol) were dissolved in DCM (10 mL) and EtOH (2 mL) and stirred at room temperature overnight. The mixture was concentrated under vacuum pump and wash with diethyl ether (20 mL) and heptane (10 mL). The precipitated compound was filtered and washed by the excess diethyl ether and heptane, affording **Ni-OH** as orange powder (0.44 g, 66.7 %). ESI-MS (positive-ion mode): *m/z* 719.2334 ($[M - Cl]^+$). Calcd: *m/z* 719.2316. Anal. Calcd for $C_{45}H_{42}N_2ONiCl_2$ (756.44): C, 71.45; H, 5.60; N, 3.70. Found: C, 71.33; H, 5.27; N, 3.71.

Ni-FOH

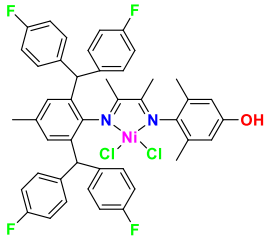

Based on the similar procedure and molar ratios described for **Ni-OH**, **Ni-FOH** was isolated as orange powder (0.51 g, 62.2 %). ESI-MS (positive-ion mode): *m/z* 791.1930 ($[M - Cl]^+$). Calcd: *m/z* 791.1957. Anal. Calcd for $C_{45}H_{38}F_4N_2ONiCl_2$ (828.40): C, 65.25; H, 4.62; N, 3.38. Found: C, 65.36; H, 4.66; N, 3.21.

Ni-PhOH

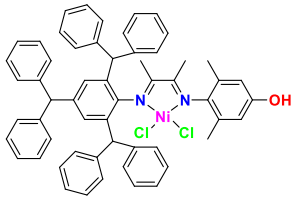

Based on the similar procedure and molar ratios described for **Ni-OH**, **Ni-PhOH** was synthesized as orange powder (0.25 g, 92.5 %). ESI-MS (positive-ion mode): *m/z* 871.3008 ($[M - Cl]^+$). Calcd: *m/z* 871.2960. Anal. Calcd for $C_{57}H_{50}N_2ONiCl_2$ (908.63): C, 75.35; H, 5.55; N, 3.08. Found: C, 75.00; H, 5.78; N, 2.81.

Ni-PhFOH

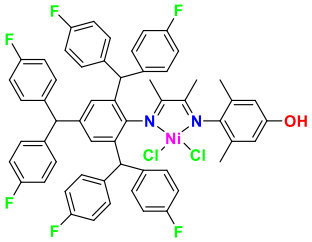

Based on the similar procedure and molar ratios described for **Ni-OH**, **Ni-PhFOH** was synthesized as yellow powder (0.66 g, 81.5 %). ESI-MS (positive-ion mode): *m/z* 472.1342 ($[M - 2Cl]^{2+}$). Calcd: *m/z* 472.1350. Anal. Calcd for $C_{57}H_{44}F_6N_2ONiCl_2$ (1016.58): C, 67.35; H, 4.36; N, 2.76. Found: C, 67.06; H, 4.39; N, 2.52.

2.4. X-ray crystallographic study

Ni-OH: Single crystals of $C_{45}H_{42}Cl_2N_2NiO$ [Ni-OH] were crystallized. A suitable crystal was selected and mounted on a STOE IPDS 2 diffractometer. The crystal was kept at 173(2) K during data collection. Using Olex2, the structure was solved with the SIR2008 structure solution program using Direct Methods and refined with the SHELXL refinement package using Least Squares minimization [50–52]. **Crystal Data** for $C_{45}H_{42}Cl_2N_2NiO$ (M = 756.41 g/mol): monoclinic, space group $P2_1/c$ (no. 14), a = 18.926(3) Å, b = 9.4716(10) Å, c = 21.408(4) Å, β = 100.789(13)°, V = 3769.8(10) Å^3, Z = 4, T = 173(2) K, μ(MoKα) = 0.694 mm^{-1}, *Dcalc* = 1.333 g/cm^3, 22,350 reflections measured (3.874° ≤ 2Θ ≤ 50.416°), 6702 unique (R_{int} = 0.0791, R_{sigma} = 0.0541) which were used in all calculations. The final R_1 was 0.0438 (I > 2σ(I)) and wR_2 was 0.1274 (all data shown in Table S1.). Supplementary crystallographic data (CCDC 2202319) is available free of charge from The Cambridge Crystallographic Data Centre CCDC.

Ni-FOH: Ni-FOH was characterized by the similar procedure for Ni-OH. **Crystal Data** for $C_{45.5}H_{39}Cl_3F_4N_2NiO$ (M = 870.84 g/mol): orthorhombic, non-centrosymmetric space group $P2_12_12$ (no. 18) with Flack −0.01(1), a = 22.900(2) Å, b = 19.6803(17) Å, c = 10.5741(7) Å, V = 4765.5(7) Å^3, Z = 4, T = 173(2) K, μ(MoKα) = 0.624 mm^{-1}, *Dcalc* = 1.214 g/cm^3, 30,791 reflections measured (2.728° ≤ 2Θ ≤ 50.368°), 8293 unique (R_{int} = 0.0549, R_{sigma} = 0.0400) which were used in all calculations. The final R_1 was 0.0468 (I > 2σ(I)) and wR_2 was 0.1448 (all data shown in Table S1.). Supplementary crystallographic data (CCDC 2202320) is available free of charge from The Cambridge Crystallographic Data Centre CCDC.

Ni-PhFOH: Ni-PhFOH was characterized by the similar procedure for Ni-OH. **Crystal Data** for C58H46Cl4F6N2NiO (M = 1101.48 g/mol): monoclinic, non-centrosymmetric space group *Cm* (no. 8) with Flack 0.01(1), a = 10.6554(12) Å, b = 18.6022(16) Å, c = 13.4204(14) Å, β = 95.166(9)°, V = 2649.3(5) Å3, Z = 2, T = 173 K, μ(Mo Kα) = 0.631 mm^{-1}, Dcalc = 1.381 g/cm^3, 18,123 reflections measured (3.048° ≤ 2Θ ≤ 51.508°), 4991 unique (R_{int} = 0.0805, R_{sigma} = 0.0488) which were used in all calculations. The final R1 was 0.0466 (I > 4u(I)) and w*R*2 was 0.1218 (all data). A solvent mask was calculated and 74 electrons were found in a volume of 216A^3 in 2 voids per unit cell. This is consistent with the presence of one heptane molecule per formula unit which accounts for 58 electrons per unit cell. (All data shown in Table S1.). Supplementary crystallographic data (CCDC 2202318) is available free of charge from The Cambridge Crystallographic Data Centre CCDC.

2.5. Polymerization procedure

The polymerization reactions were carried out in a 300 mL stainless *Büchi* steel autoclave. The polymerization setup was equipped and connected with multifunctional systems including vacuum, argon pipeline, monomer feeding tank, catalyst injection, temperature control, and magnetic stirrer with controlling units. The temperature inside the reactor was controlled by the connected thermostat. The reactor was initially vacuumed and filled up with argon for three time. The desired amount of mixture of dry solvent (toluene) and co-catalysts was injecting inside to wash and clean the impurities in the reactor. The washing procedure was maintained for 15 min under 90 ℃. Then, the solution mixture was released by the argon pressure, which kept the inert atmosphere in reactor. At the selected polymerization conditions, the distill toluene (30 mL) was injected into the autoclave, followed by the injection of co-catalyst dissolved in dry toluene (50 mL). Ni complexes were purified using the *Schlenk* manipulations under argon. The required amount of Ni complexes was introduced with dissolution of the

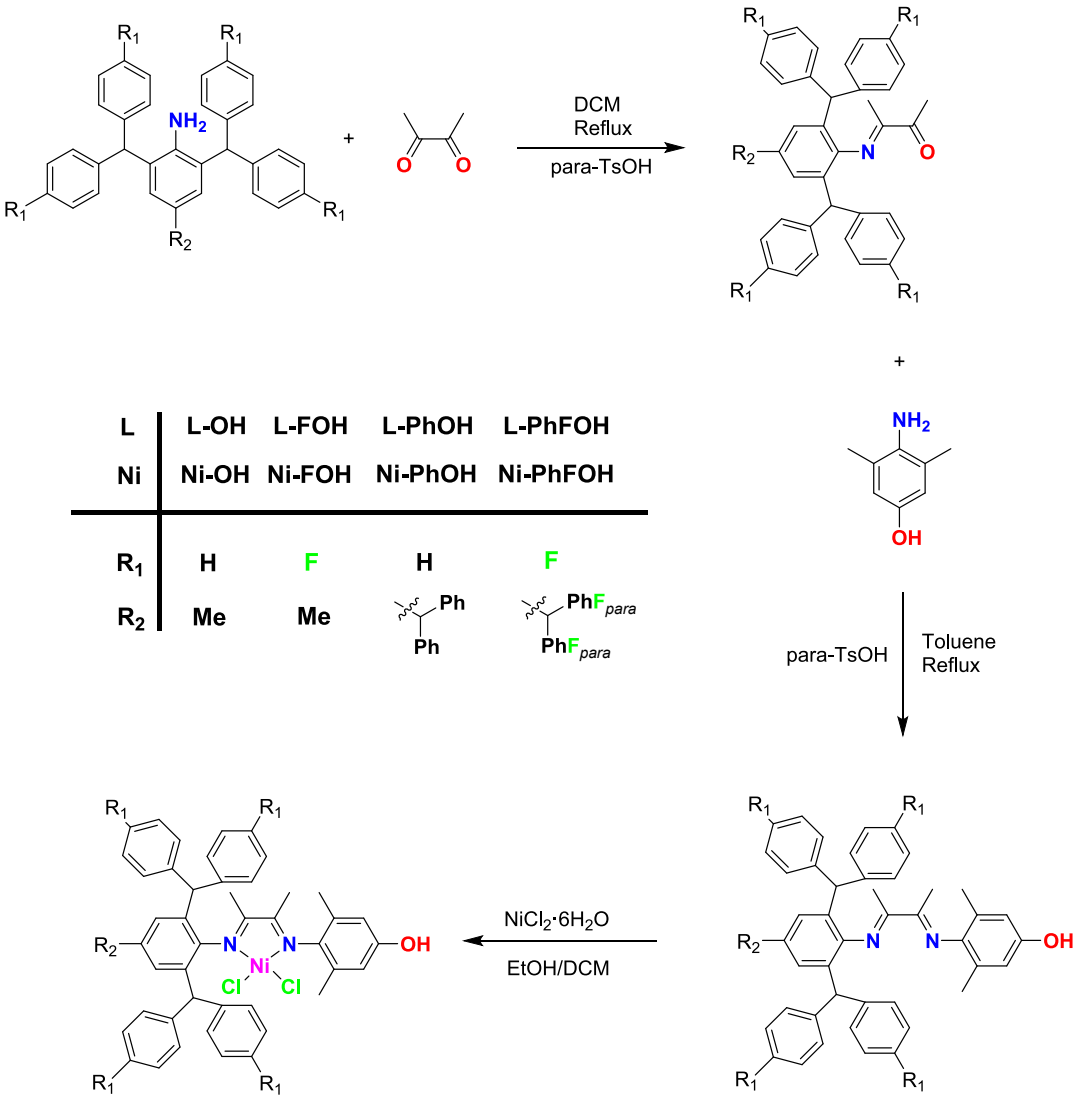

Fig. 2. Synthesis route on the new *a*-diimine ligands and corresponding Ni(II) complexes.

rest 20 mL toluene. The reactor was immediately pressurized into certain ethylene pressure while the magnetic stirrer was also initiated at the same time. After the required time for ethylene polymerization, the monomer pressure was released out of the autoclave. The mixed solution containing polymers was removed out and quenched by the mixture of HCl and EtOH (ratio 1:10). The polymer was collected, washed with EtOH, and then dried under vacuum oven at 60℃ for further catalytic calculation and characterization.

3. Result and discussion

3.1. Synthesis and characterization of a-diimine ligands and Ni complexes

The synthesis of the here proposed *a*-diimine Ni complexes could be divided into several parts, namely the synthesis of bulky anilines, *a*-imino-ketones, *a*-diimine ligands and Ni complexes (Fig. 2). The synthetic procedure of the bulky anilines has previously been reported, which involved the reaction between the normal anilines and diphenylmethanol catalyzed by zinc chlorides [53–55]. Subsequently, one-equivalent 2, 3-butanedione reacted with these bulky anilines with a catalytic amount of *para*-toluene sulfonic acid in dichloromethane under reflux, producing the *a*-imino-ketone precursors. The unsymmetrical *a*-diimine ligands were synthesized via the imine formation reaction of *a*-imino ketones with 4-amino-3,5-xylenol. The most conventional starting material for the synthesis of *a*-diimine Ni(II) complexes is the nickel(II) bromide 2-methoxyethyl ether complex ((DME)$NiBr_2$) [11]. As (DME) $NiBr_2$ is very sensitive to moisture, the synthesis of *a*-diimine Ni complexes has to be carried out under inert atmosphere. The aid of air-stable nickel(II) chloride hexahydrate ($NiCl_2{\cdot}6H_2O$) as the coordination affiliation is rarely reported [17]. Additionally, the price of (DME)$NiBr_2$ is even higher than $NiCl_2{\cdot}6H_2O$. The inert-protection procedure during the synthesis and the high price of chemicals definitely increases the catalyst cost, which hampers their commercialization. Therefore, the more efficient and cheaper $NiCl_2{\cdot}6H_2O$ was applied to produce the *a*-diimine Ni chlorides in ethanol/DCM mixture, which was completely carried out at ambient. The components of the *a*-diimine ligands and Ni complexes synthesized in this work are not commercially available, nor was their synthesis reported previously.

The *a*-diimine ligands (**L-OH**, **l-FOH**, **L-PhOH,** and **L-PhFOH**) were characterized by elemental analysis, ^{1}H, ^{13}C, and ^{19}F NMR spectroscopy (Figs. S1–S10). The NMR analysis was also employed to verify the *a*-diimine Ni (II) complexes (**Ni-OH**, **Ni-FOH**, **Ni-PhOH,** and **Ni-PhFOH**). However, owing to the paramagnetic behavior of the Ni based complexes, the chemical shifts of the ^{1}H NMR signals were very broad and difficult to determine their complex structures comparing to the ligands (Figs. S11–S14) [56]. As a consequence, the *a*-diimine Ni (II) complexes

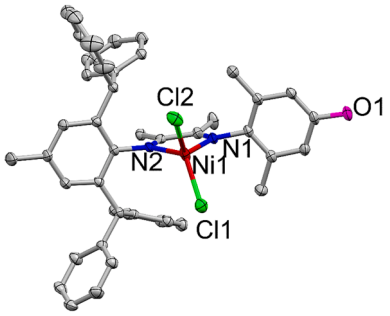

Fig. 3. Single-crystal structure of **Ni-OH** drawn with 30% probability ellipsoids. Hydrogen atoms were omitted for clarity. Selected bond length (Å): Ni1—Cl1: 2.2325(9), Ni1—Cl2: 2.1840(10), Ni1—N1: 1.982(2), Ni1—N2: 2.0076(19), N1—C1: 1.451(3), N2—C13: 1.446(3); selected angle (°): N1—Ni1—N2: 80.72(8), Cl1—Ni1—Cl2: 119.28(3), N1—Ni—Cl1: 108.06(7), N2—Ni—Cl1: 120.09(6), N1—Ni—Cl2: 116.67(6), N2—Ni—Cl2: 106.22(6).

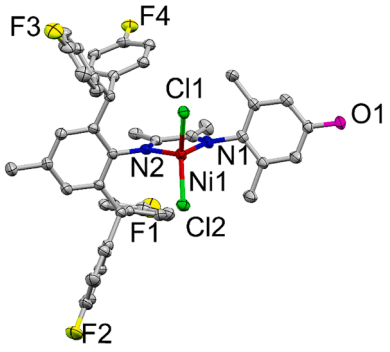

Fig. 4. Single-crystal structure of **Ni-FOH** drawn with 30% probability ellipsoids. Hydrogen atoms were omitted for clarity. Selected bond length (Å): Ni1—Cl1: 2.2295(17), Ni1—Cl2: 2.1881(17), Ni1—N1: 1.990(5), Ni1—N2: 1.987(5), N1—C1: 1.453(7), N2—C13: 1.427(7); selected angle (°): N1—Ni1—N2: 80.72(8), Cl1—Ni1—Cl2: 125.50(6), N1—Ni—Cl1: 103.82(15), N2—Ni—Cl1: 111.00(15), N1—Ni—Cl2: 117.04(17), N2—Ni—Cl2: 109.21(14).

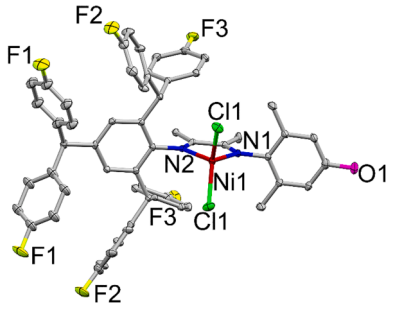

Fig. 5. Single-crystal structure of **Ni-PhFOH** drawn with 30% probability ellipsoids. Hydrogen and were omitted for clarity. Selected bond length (Å): Ni1—Cl1: 2.2071(15), Ni1—Cl2: 2.2071(15), Ni1—N1: 2.013(5), Ni1—N2: 2.026(6), N1—C5: 1.438(9), N2—C10: 1.430(9); selected angle (°): N1—Ni1—N2: 81.2(2), Cl1—Ni1—Cl2: 126.68(9), N1—Ni—Cl1: 110.27(7), N2—Ni—Cl1: 109.57(7), N1—Ni—Cl2: 110.27(7), N2—Ni—Cl2: 109.57(7).

were further characterized by Elemental Analysis, ESI-HRMS, and a single-crystal X-ray diffraction study. Particularly, the single crystals of **Ni-OH**, **Ni-FOH**, and **Ni-PhFOH** were isolated from slow-diffusion of heptane (nonpolar solvent) into a dichloromethane solution (polar solvent) and further verified via X-ray crystallographic analysis. It was also found that storage in the solvents was critical to protect the single-crystals from decomposition. The molecular structures of the

Table 1
Ethylene polymerization using various co-catalysts and **Ni-FOH**.[a]

Entry	Co-catalyst	Al/Ni	Yield, g	Act.[b]	M_w[c]	M_w/M_n[c]	T_m[d], °C
1	MMAO	2000	2.17	13.02	1.36	2.5	108.4
2	EASC	500	2.12	12.72	0.71	2.1	67.9
3	Et_2AlCl	500	1.47	8.82	0.77	2.4	73.7
4	TMA	500	traces	–	–	–	–

[a] General conditions: 1 μmol of **Ni-FOH**; 30 °C; 10 min; 10 bar of ethylene gas (constant flow); 100 mL total volume of anhydrous toluene, 3000 r/min.
[b] Unit of 10^6 g of PE (mol of Ni)$^{-1}$ h^{-1}.
[c] Unit of 10^6 g mol^{-1}, determined by GPC in 1,2,4-trichlorobenzene at 160 °C versus linear polystyrene standards.
[d] Determined by DSC (second heating scan).

complexes are shown in Figs. 3–5 with selected bond lengths and angles. In the Ni complexes, the Ni atom is situated at the center of a distorted-tetrahedron structure. Two nitrogen donors belonging to the unsymmetrical *α*-diimine ligands coordinate with Ni chlorides. The two *N*-aryls are perpendicular to the planar coordination sphere of Ni and aliphatic backbone. The phenyl rings of the *N*-aryls surround the coordinated Ni center, which partially shields it and controls the monomer insertion rates. Thus via the various steric and electronic effects, the coordination environment is finely tuned, as evidenced by the variation of bond lengths and bond angles among these different Ni complexes. The characteristic tetrahedral geometry of *α*-diimine Ni (II) complexes favors the improved catalytic activity in catalyzed ethylene polymerization [57].

3.2. Ethylene polymerization

As a first step, the initiating effects of different activators (co-catalysts) were screened for the *in situ* polymerization using the synthesized Ni complexes. Numerous alkyl-aluminum compounds have been previously reported as activators for late-transition metal precatalysts [17]. In this work, initiation effect of various activators such as modified methylaluminoxane (MMAO), ethylaluminum sesquichloride (EASC), diethylaluminumchloride (Et_2AlCl), and trimethylaluminium (TMA) were studied. Although the activation mechanism of these co-catalysts might be slightly different, the monomer insertion of ethylene into the active cationic alkyl-metal species remains the same. The screening of co-catalyst initiation were performed using **Ni-FOH** in toluene with a constant ethylene pressure of 10 bar and a temperature of 30 °C (see Table 1).

As shown in Table 1, all co-catalysts except TMA exhibited remarkable capacity to initiate **Ni-FOH**. MMAO is the most efficient activator for **Ni-FOH** in ethylene polymerization resulting in a catalytic activity of 13.0 × 10^6 g of PE (mol of Ni)$^{-1}$ h^{-1}. Furthermore, the GPC analysis revealed the high molecular weight (1.36 × 10^6 g mol^{-1}) for the isolated PE in the MMAO-**Ni-FOH** system (see entry 1, Table 1). High activities were also observed for the Et_2AlCl-**Ni-FOH** and EASC-**Ni-FOH** system (12.7 and 8.8 × 10^6 g of PE (mol of Ni)$^{-1}$ h^{-1}) (entries 2 and 3, Table 1). However, the molecular weight of the PE decreased for Et_2AlCl and EASC compared to the MMAO-**Ni-FOH** system. This particularly demonstrates the competition between the chain-growth and chain-transfer process [58]. The latter led to a decrease in the molecular weight of PE. Somehow, the Et_2AlCl-**Ni-FOH** and EASC-**Ni-FOH** system seemed to provide the active species, which typically favored the chain-transfer process in ethylene polymerization. TMA is not a suitable activator for the **Ni-FOH** complex (entry 4, Table 1). Nevertheless, the main cause of this poor activation performance of TMA-**Ni-FOH** still remains unclear. As previously reported, TMA was also applied as the significant linker to covalently tether the OH/NH_2-containing late-transition complexes to solid substrate for ethylene heterogeneous polymerization [59,60]. It is also likely that TMA reacts with the Ni complex (**Ni-FOH**) and generates the *α*-diimine Ni dimethyl or heterobinuclear Ni(I) species, rather than initiating the catalytic metal center for polymerization [61].

Table 2
Ethylene polymerization conditions with various Ni precatalysts and polymer characteristics.[a]

Entry	Ni	Al/Ni	T, °C	t, min	P^{b}	Yield, g	Act.[c]	M_w[d]	M_w/M_n[d]	T_m[e], °C
1	**Ni-FOH**	500	30	10	10	1.56	9.36	1.36	2.0	107.1
2	**Ni-FOH**	1000	30	10	10	2.76	16.56	1.20	2.2	113.1
3	**Ni-FOH**	1500	30	10	10	3.64	21.84	1.38	2.0	106.7
4	**Ni-FOH**	2000	30	10	10	2.17	13.02	1.36	2.5	108.4
5	**Ni-FOH**	2500	30	10	10	1.24	7.44	1.22	2.3	106.4
6	**Ni-FOH**	1500	0	10	10	0.48	2.88	1.81	1.7	127.5
7	**Ni-FOH**	1500	60	10	10	0.83	4.98	0.53	2.5	116.2
8	**Ni-FOH**	1500	90	10	10	0.47	2.82	0.45	4.9	116.1
9	**Ni-FOH**	1500	30	5	10	2.31	27.72	0.98	2.2	118.3
10	**Ni-FOH**	1500	30	15	10	4.30	17.20	1.29	2.2	112.2
11	**Ni-FOH**	1500	30	30	10	6.33	12.66	0.96	2.3	111.5
12	**Ni-FOH**	1500	30	60	10	10.13	10.13	1.02	2.1	114.5
13	**Ni-FOH**	1500	30	120	10	15.13	7.57	1.09	2.2	121.7
14	**Ni-FOH**	1500	30	10	5	1.87	11.22	1.16	2.8	109.8
15	**Ni-FOH**	1500	30	10	15	4.05	24.30	1.29	2.8	120.6
16	**Ni-FOH**	1500	30	10	20	4.85	29.10	1.53	2.6	123.2
17	**Ni-OH**	1500	30	10	10	1.45	8.70	1.15	2.4	105.8
18	**Ni-PhOH**	1500	30	10	10	2.05	12.30	1.52	2.1	109.5
19	**Ni-PhFOH**	1500	30	10	10	3.95	23.70	1.71	1.9	107.0
20	**Ni-OH**	1500	90	10	10	0.45	2.70	0.63	5.6	111.4
21	**Ni-PhOH**	1500	90	10	10	0.38	2.28	0.86	8.1	114.8
22	**Ni-PhFOH**	1500	90	10	10	0.36	2.16	0.84	7.2	115.3

[a] General conditions: 1 μmol of **Ni** precatalysts; co-catalyst: MMAO; 100 mL total volume of anhydrous toluene, 3000 r/min.
[b] Bar of ethylene gas (constant flow).
[c] Unit of 10^6 g of PE (mol of Ni)$^{-1}$ h^{-1}.
[d] Unit of 10^6 g mol^{-1}, determined by GPC in 1,2,4-trichlorobenzene at 160 °C versus linear polystyrene standards.
[e] Determined by DSC (second heating scan).

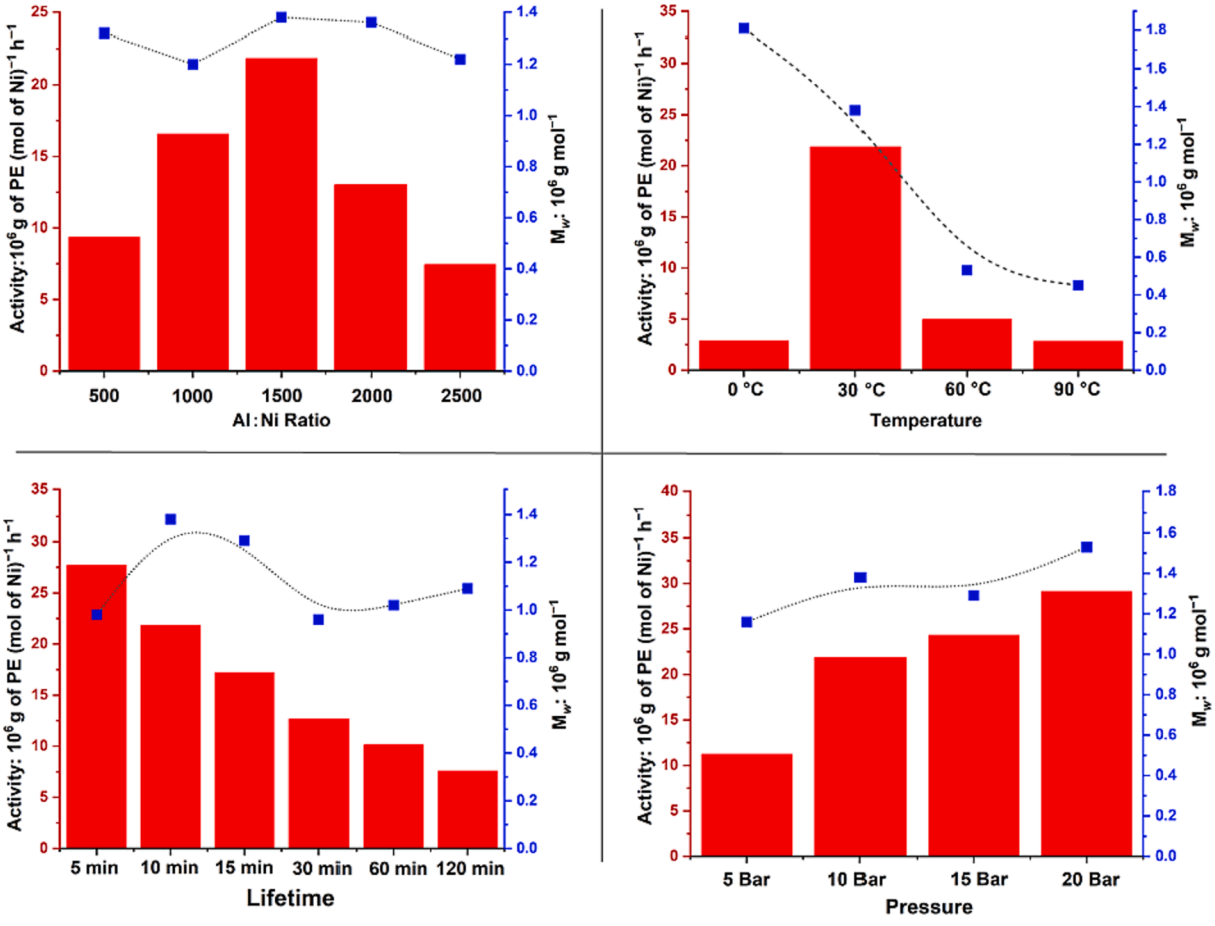

Fig. 6. Catalytic activity and molecular weight for optimized conditions.

Furthermore, the influence of various polymerization conditions, such as Al: Ni ratio, polymerization temperature, catalyst lifetime and ethylene pressure, for the MMAO-**Ni-FOH** catalytic system was investigated to improve the catalyst's performance (entries 1–16, Table 2 and Fig. 6). Initially, the influence of the Al: Ni molar ratio was optimized with an ethylene pressure of 10 bar, a polymerization time of 10 min and a polymerization temperature of 30 °C (entries 1–5, Table 2). The catalytic activities of the systems displayed an upward trend as the ratio was increased from 500: 1 to 1500: 1. The highest activity (21.84 × 10^6 g (PE) mol^{-1} (Ni) h^{-1}) was observed at a molar ratio of 1500: 1. Above this molar ratio, the catalytic activity steadily dropped to 7.44 × 10^6 g (PE) mol^{-1} (Ni) h^{-1} (Fig. 6). This decreased activity was plausibly attributed to the presence of the —OH moiety in the *para-N*-aryl, as higher Al: Ni molar ratios generates —O^- ions from —OH. These —O^- ions are strong electron-donating group, which weaken the catalytic capacity of the Ni centers [62]. All PE samples exhibited the high molecular weight, typically around 1.2–1.3 × 10^6 g mol^{-1}. However, no obvious correlation between the PE molecular weights and the catalyst activity was observed.

The effect of temperature on the performance of the MMAO-**Ni-FOH** system was tested by conducting polymerization under selected temperature gradients with a constant Al: Ni ratio of 1500:1 (entries 3, 6–8, Table 2). It was observed that the reaction temperature had a significant influence on the catalytic activity and the molecular weight (Fig. 6) of the PE; namely, the molecular weight diminished (from 1.81 to 0.45 × 10^6 g mol^{-1}) with increased temperatures. The MMAO-**Ni-FOH** system achieved the highest activity of 21.84 × 10^6 g (PE) mol^{-1} (Ni) h^{-1} at 30 °C. A high molecular weight for the formed PE at 0 °C was attributed to the low rate rotation of the C-*N*-aryl bond and chain transfer, which decreased the rate of the monomer insertion and activity [63]. Along with a higher activity and molecular weight, a better balance between the chain propagation and chain transfer mechanism could be achieved at 30 °C. As expected, both catalytic activity and the molecular weight decreased significantly at higher polymerization temperatures (60 and 90 °C). A persuasive explanation can be made that the increased temperature gave rise to the increased rotation of C-*N*-aryl bond. High rate rotation of the C-*N*-aryl bond led to the fast chain transfer (low M_w) and thermal damages to the metal center (chain termination). A polymerization temperature of 90 °C yielded an activity of 2.8 × 10^6 g (PE) mol^{-1} (Ni) h^{-1} and a molecular weight of 0.4 × 10^6 g mol^{-1} (entry 8, Table 2). Meanwhile, higher temperature also reduced the concentration of the ethylene monomer in toluene solution, therefore decreasing the monomer access. However, the catalytic performance of **Ni-FOH**/MMAO also suggests great thermal stability compared to systems reported in previous works [17].

Additionally, variation of the polymerization time was used to check the lifetime of the activated Ni species (entries 3, 9 – 13, Table 2). As shown in Fig. 6, the highest activity (27.7 × 10^6 g (PE) mol^{-1} (Ni) h^{-1}) was achieved around 5 min after the beginning of the polymerization; then the activity gradually decreased from 5 min to 120 min, leading to 7.7 × 10^6 g (PE) mol^{-1} (Ni) h^{-1}. The reason for this decrease might be due to a monomer diffusion limit. As the synthesized PE was not fully dissolved in toluene, a polymeric diffusion barrier around the metal center was created during the ethylene polymerization. This reduced the possibility of the coordination-insertion process between the Ni center and ethylene monomer. There is the possibility that the Ni complexes were partially deactivated during the long-term polymerization. However, the catalytic activity of the Ni complexes was still maintained at high level even after 2-hour reactions, demonstrating the robust nature of these synthesized catalysts. To further investigate the influence of ethylene pressure, polymerizations were performed between 5 and 20 bar (entries 3, 14 – 16, Table 2), as a higher monomer pressure leads to a higher ethylene concentration in toluene solution. Consequently, higher activity (up to 29.1 × 10^6 g (PE) mol^{-1} (Ni) h^{-1}) and molecular weight (M_w = 1.53 × 10^6 g mol^{-1}) were observed at 20 bar (Fig. 6). This result demonstrates a superior performance of the catalyst under increased polymerization pressure.

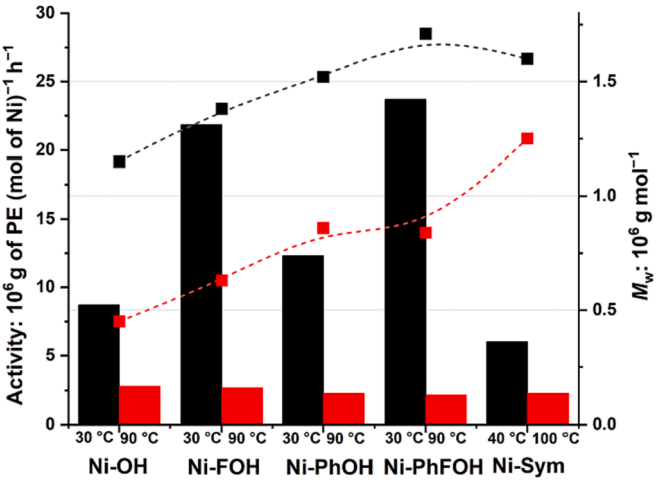

Fig. 7. Comparison on Catalytic activity and PE molecular weight of various *α*-diimine Ni complexes.

The structural modifications of the *α*-diimine Ni complexes were of significant importance to control the catalytic behavior and the properties of the synthesized PE. In order to determine the catalytic performance, **Ni-OH**, **Ni-FOH**, **Ni-PhOH**, and **Ni-PhFOH** were applied to the ethylene polymerization under the previously optimized conditions (entries 3, 17 – 22, Table 2). All the Ni complexes exhibited a high catalytic (8.7 – 23.7 × 10^6 g (PE) mol^{-1} (Ni) h^{-1}) activity for ethylene polymerization at 30 °C. It was apparently observed that the F effect and the incorporation of the sterically demanding groups generated positive influences on the catalytic activity and molecular weight of the resulting PE. Both, **Ni-FOH** and **Ni-PhOH** exhibited higher catalytic activity compared to **Ni-OH,** whereas the catalytic activity of **Ni-FOH** was also higher than **Ni-PhOH**. These findings together indicated that the F effect plays a crucial role in improving the catalytic activity at 30 °C. The highest activity of these Ni complexes was achieved using **Ni-PhFOH** as the pre-catalysts, probably due to the combination of the F effects and the steric enhancement (Fig. 7). There was a trend concerning the molecular weight of the produced PE for different ligand structures: **Ni-PhFOH** (1.71 × 10^6 g mol^{-1}) > **Ni-PhOH** (1.52 × 10^6 g mol^{-1}) > **Ni-FOH** (1.38 × 10^6 g mol^{-1}) > **Ni-OH** (1.15 × 10^6 g mol^{-1}) observed, which could be understood as follows. The restricted access from axial directions of the metal center suppressed the chain-transfer process more efficiently, which leads to a further increase of molecular weight via chain propagation. However, the F and steric effects did not have a great impact on the catalytic activity of the Ni complexes at 90 °C. Although the catalytic performance was maintained at high activity [> 10^6 g (PE) mol^{-1} (Ni) h^{-1}], a minor decrease was nevertheless observed for all Ni complexes (Fig. 7) – probably due to a boost of the rotation rate of the C-*N*-aryl bond at the high reaction temperature. The coordination between the protons from the alkyl-*N*-aryl groups and the metal center terminated the catalytic active species. The presence of the -$CHPh_2$ groups at the *para-N*-aryl led to an increase in the molecular weight of PE, thus **Ni-PhFOH** and **Ni-PhOH systems** yielded a higher molecular weight PEs compared to **Ni-FOH** and **Ni-OH** systems. Compared to the symmetrical modifications on α-diimine Ni complexes with the incorporation of the 2, 6-dibenzhydryl groups (**B** in Fig. 1), one of the biggest advantages of the proposed Ni complexes (**Ni-PhFOH**, **Ni-PhOH**, **Ni-FOH** and **Ni-OH**) is the remarkably high catalytic activity in ethylene polymerization [21,22]. Even after 1 h, the catalytic activity was still maintained at the level of 10^7 g (PE) mol^{-1} (Ni) h^{-1} (entry 11, Table 2). Derivative **Ni-*Sym*.** from a previous research [46]. similar to **B** [21,22]. was selected as a benchmark reference for this work (as shown in Fig. 7). The steric bulkiness of both sides of the *N*-aryls limited the space for monomer insertion, thus reducing the catalytic activity. Furthermore,

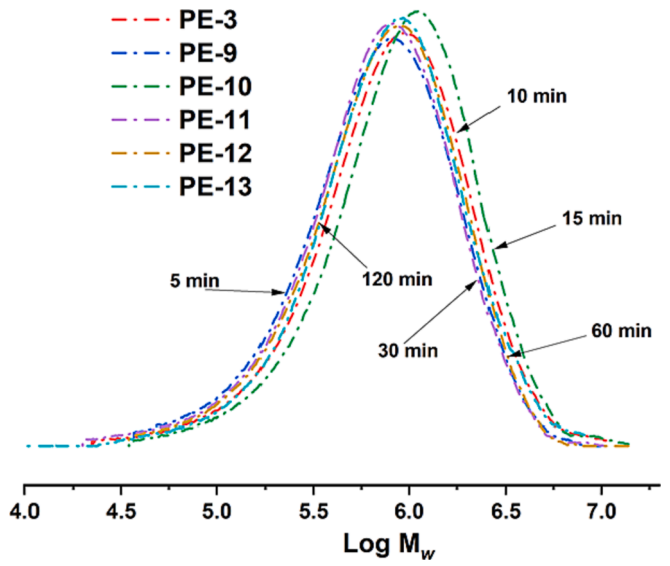

Fig. 8. GPC traces on the different run times of the resultant PE (Table 2) obtained using **Ni-FOH**/MMAO catalytic system (PE-No. is defined as the polyethylene produced from specific entry in Table 1 or 2, same as below).

the rigid structure of the symmetrical Ni complexes also created fewer opportunities to modify the molecular weights and other properties of the resulting PE. Contrary to this, the unsymmetrical designs of the *α*-diimine Ni complexes (**Ni-PhFOH**, **Ni-PhOH**, **Ni-FOH**, and **Ni-OH**) offered both a tailored catalytic activity and a high molecular weight PE (Fig. 7). Meanwhile, this work combines the excellent catalytic features of previously described unsymmetrical *α*-diimine Ni complexes [64–69]. The incorporation of the aliphatic backbone is more likely to generate the PE samples with higher Mw (up to 1.81 × 10^6 g mol^{-1}) in comparison to the aromatic backbone. A high catalytic activity and thermal stability of such unsymmetrical *α*-diimine Ni complexes were also observed in this work. Compared to the previous derivatives with aliphatic backbone, the steric enhancements on both the para- and *ortho*-position of the *N*-aryls allows for generation of a stable single-site catalytic Ni center during the ethylene polymerization[69]. In the current work a high catalytic activity, high PE Mw and narrow PDI were observed. In addition, the presence of the terminal hydroxyl group offers reactive site for covalent immobilization of these outstanding *α*-diimine Ni complexes on inorganic substrates for applications in heterogeneous polymerization.

3.3. Polymer microstructure

Compared to the currently applied *Ziegler-Natta* heterogeneous catalysis in ethylene polymerization, one of the main advantages of single-site catalysts is the formation of PE with narrow molecular weight distribution. As shown in Fig. 8, the PE samples catalyzed by the *α*-diimine Ni complexes typically exhibit a narrow PDI, enabling better mechanical properties of the resultant polymer [70]. However, broader PDIs (higher than 3) were observed for the PE samples generated at a polymerization temperature of 90 °C for all the Ni complexes. It illustrates that deactivation and chain termination occurs at higher temperatures during ethylene polymerization.

In addition, the steric hindrance from the *para*-*N*-aryl potentially squeezed the free volume of the phenyl rings at the *ortho*-*N*-aryl, which increased the possibility for the coordination between the C—H and the active Ni centers [71]. Besides a narrow PDI, branched structure is another potential advantage of the *α*-diimine Ni complexes, enhancing the polymer mechanical flexibility, such as the tensile strength and elongation at break [72]. The chain-walking mechanism allowed the *α*-diimine Ni and Pd complexes to produce high molecular weight PE with highly branched structures [73]. The branched microstructures of the resulting PE samples was determined by the high-temperature ^{1}H

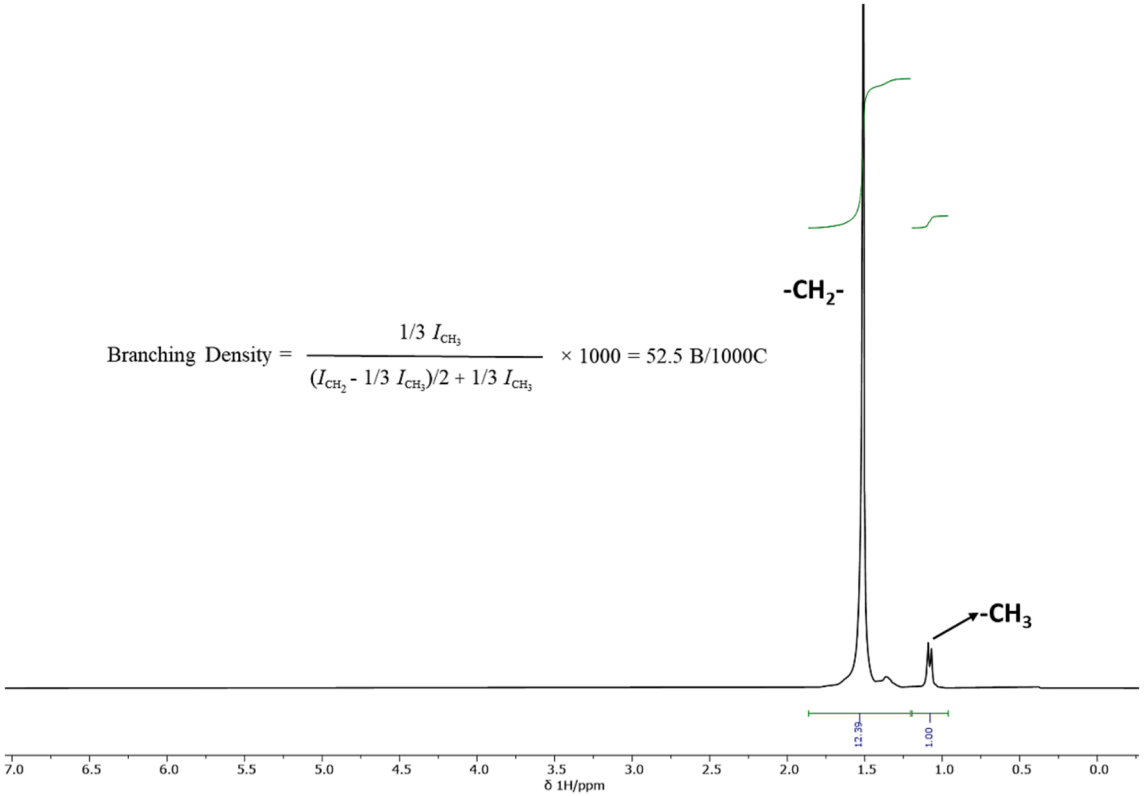

Fig. 9. High-temperature ^{1}H NMR spectra of **PE-3′** (Table 1) in Bromobenzene-d_5.

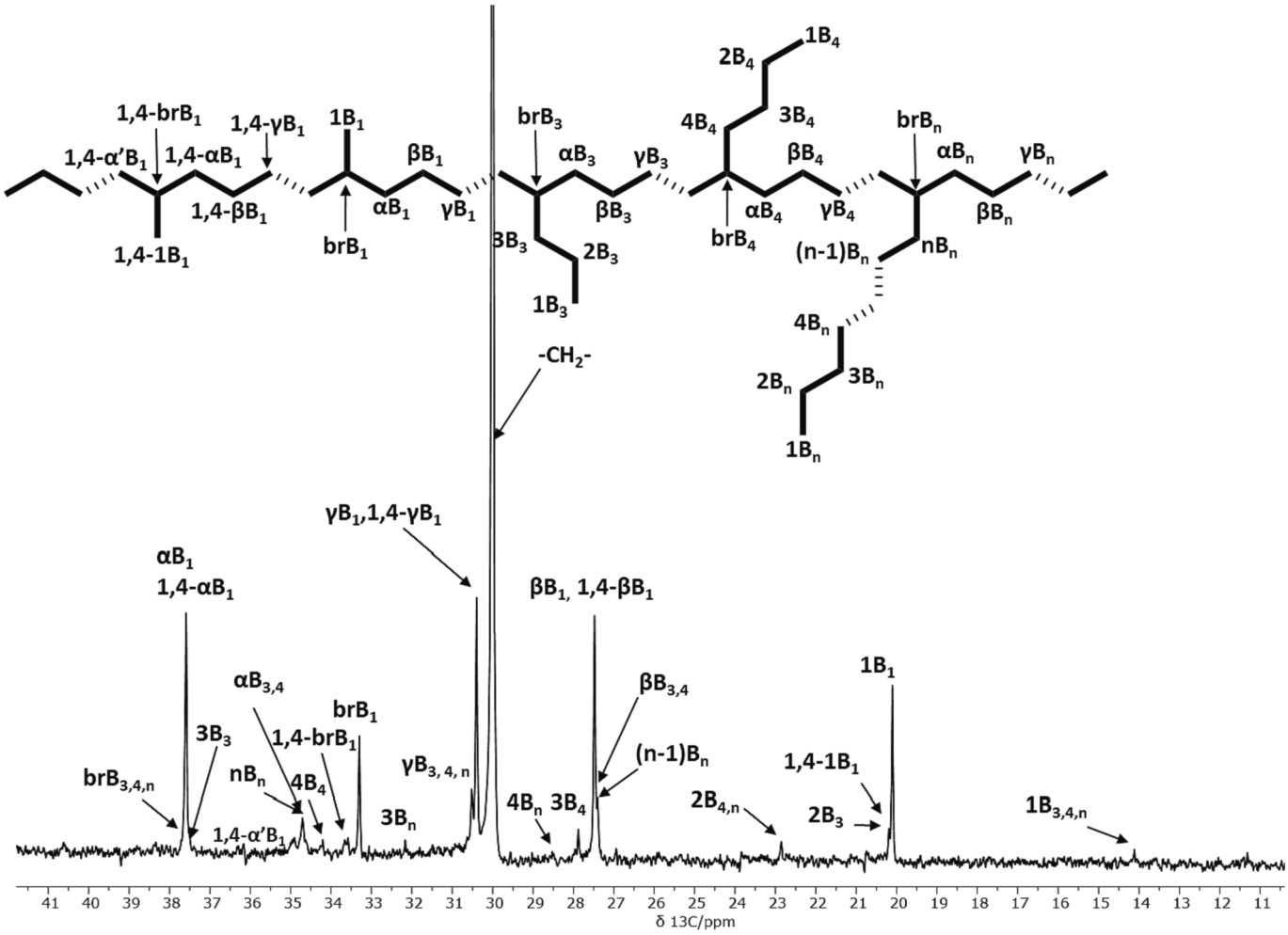

Fig. 10. High-temperature ^{13}C NMR spectra of **PE-3′** (Table 1) in Bromobenzene-d_5.

and ^{13}C NMR (Figs. 9–11).The calculation of the branching density and peak assignments of the PE simples were based on the methods, which were previously reported [19,25,74]. As shown in Fig. 9, the ^{1}H NMR spectra of the **PE-3′** sample (entry 3 in Table 1) shows a significant quantity of terminal methyl groups in the polymer chains, which is interpreted as evidence for the PE branching (52.5B/1000C). ^{13}C NMR spectra also helps to characterize various types of branching architectures. For instance, the ^{13}C NMR spectra of the **PE-3′** sample (Table 1) revealed multiple branching types in Fig. 10, including methyl (50.5 %), propyl (15.2 %), butyl (10.6 %), and long chain moieties (23.7 %). The polymer microstructure of sample **PE-3** (entry 3 in Table 2.) exhibited less variation in the branches (26.2B/1000C) than the **PE-3′** sample (Table 1).

Obviously, only methyl branches were detected in the ^{13}C NMR spectra for the **PE-3** sample (Table 2.), shown in Fig. 11. Interestingly, such branched elastomer like PE was obtained *via* ethylene polymerization in this work by using ethylene only as the monomer feedstock; remember, the difference in the synthesis of **PE-3′** (Table 1) and **PE-3** (Table 2) was the use of a different co-catalysts (Et_2AlCl or MMAO), applied for ethylene polymerization. This surprising finding suggests that the variation of the co-catalysts plays a role in altering the chain-walking behavior at the hence initiated Ni center—the exact details remaining unclear. A possible explanation could be that the co-catalysts initiation can induce the selectivity of the activated Ni center, where either the chain propagation (MMAO and **PE-3** (Table 2.) or chain transfer (Et_2AlCl and **PE-3′** (Table 1) is favored upon ethylene insertion. It was observed that the molecular weight of **PE-3** (Table 2) was almost twice as high as **PE-3′** (Table 1), also indicating a higher rate of chain transfer if activated with Et_2AlCl as compared to MMAO. Therefore, a high rate of chain transfer increased the chances of chain-walking process thus leading to the formation of branched structures. A similar observation was made in catalyzed propylene polymerization, where the MMAO activation formed a much higher syndiotacticity in comparison to the in-situ activated hafnocenes. This stereoselectivity was assumed to be attributed to the effects of counter anion [75]. Moreover, higher temperatures led to an increasing rate of the chain-walking process as well as branching, which was due to the C-*N*-aryl rotations of the Ni complexes. As shown in Fig. S15, for the **PE-8** samples (Table 2), the ^{13}C NMR spectra shows the presence of both the methyl (66 %) and propyl groups (34 %) as the branches (69.9B/1000C), if synthesized at 90 °C. The branching density of the PE sample also suggests a higher rate of the chain-transfer process as compared to **PE-3** (Table 2), which was synthesized at 30 °C [57]. The variation of the melting points was mainly due to the different branching densities and structures, which led to the formation of various crystallinity and microstructures of the PE samples. The branching properties of PE samples were directly modified by the so-called chain-walking process in ethylene polymerization, catalyzed by such Ni complexes. The competition between the chain-growth and chain-walking process can be modulated by the applied polymerization conditions or complexes structures. The higher degree of branching densities, the lower melting points are characterized (Fig. 12). For example, hyperbranched and amorphous PE can be prepared via the α-diimine Pd complexes, which exhibits higher selectivity to chain-walking process than α-diimine Ni complexes in ethylene

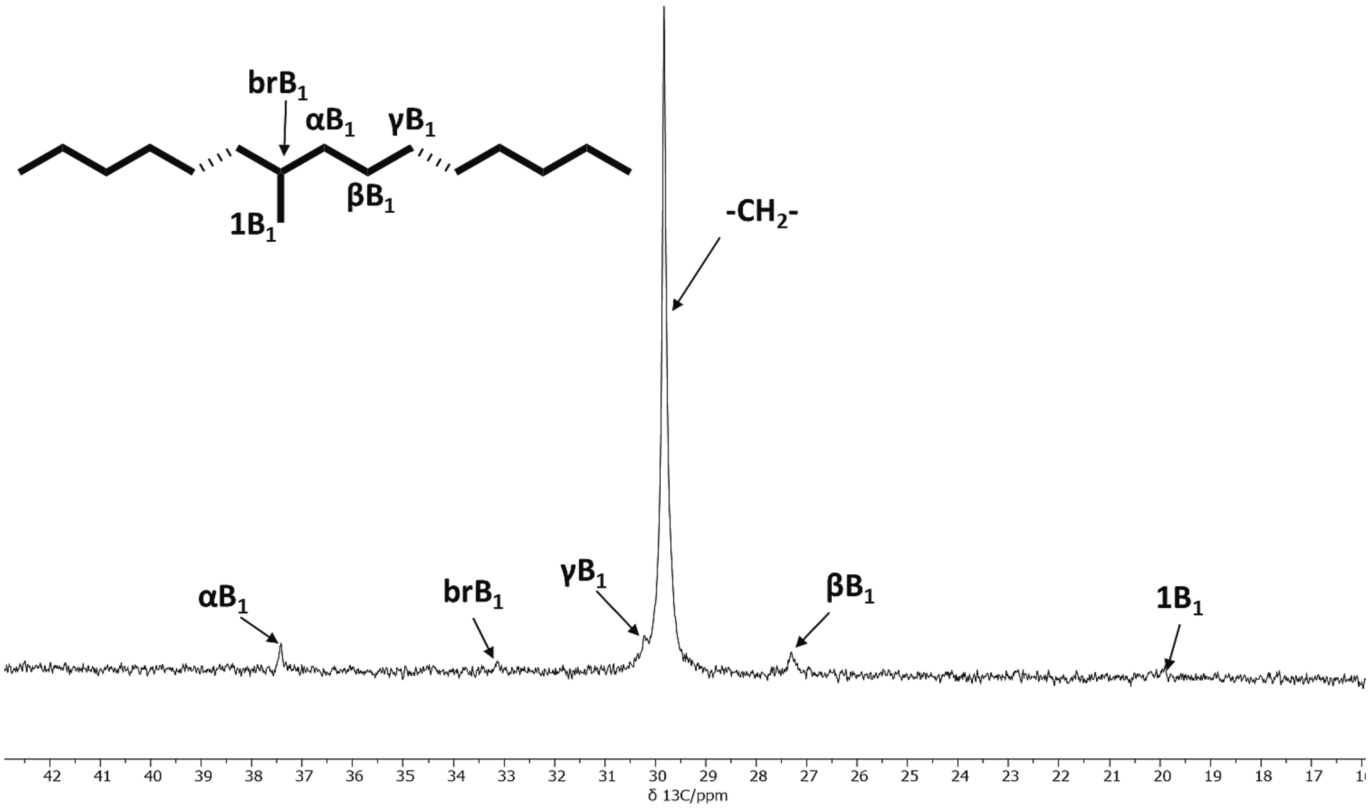

Fig. 11. High-temperature ^{13}C NMR spectra of **PE-3** (Table 2) in Bromobenzene-d_5.

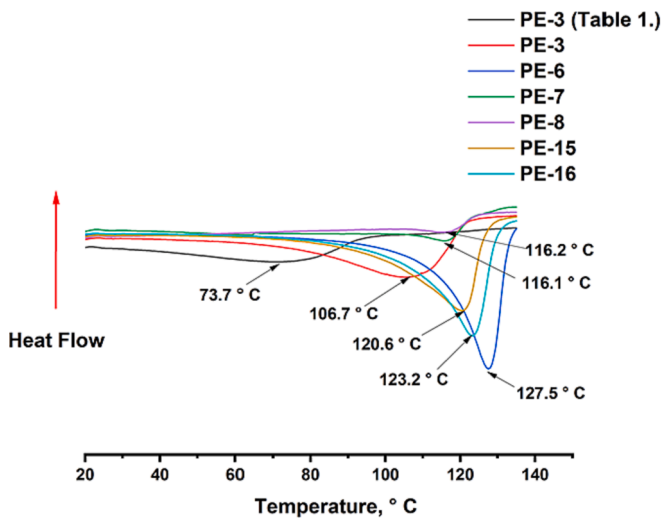

Fig. 12. DSC (Second-heating-scan) curves on the selected PE samples (Table 2, otherwise mentioned) obtained using **Ni-FOH.**

polymerization [14,20]. The α-diimine Ni complexes can produce mainly linear (few short-branches) PE with a well-defined melting point. DSC (second-heating-scan) curves revealed diverse microstructures of the selected PE samples, which were initially controlled various ligands structures and polymerization conditions. The melting points of the produced PE range from 67.9 up to 127.5 °C.

4. Conclusion

In conclusion, this work presents a series of novel unsymmetrical *α*-diimine Ni complexes for ethylene polymerization, combining the benefits of high activity and high molecular weight PE. The two unsymmetrical *N*-aryl groups created the unique coordination surroundings toward the active metal center. The dibenzhydryl groups (-$CHPh_2$/-$CHPhF_{para2}$) on *N*-aryl suppressed the axial direction of the Ni coplanar and retarded the rate of chain transfer, which gave rise to high molecular weight of polyethylene ($M_w = 1.8 \times 10^6$ g mol^{-1}). Meanwhile, the less bulky *N*-aryl provided enough space for monomer insertion, leading to the high catalytic activity (29.1×10^6 g of PE (mol of Ni)$^{-1}$ h^{-1}). The incorporation of the fluorine atoms on the bulky substitutions brought about the significant increase on the catalytic activities of these Ni complexes and PE molecular weight ($M_w = 1.7 \times 10^6$ g mol^{-1}). It also indicated that the polymerization conditions played a crucial role in controlling the catalytic behaviors and PE microstructures, including the co-catalysts, polymerization temperature and ethylene pressure. High melting transitions (up to 127.5 °C) were observed among the selected PE samples. The presence of the strong electro-donating hydroxyl group at the *para*-*N*-aryl did not negatively influence the catalytic activity, while it provided the opportunities to further functionalized the newly synthesized *α*-diimine Ni complexes. These unique unsymmetrical structures must generate a gradient polarizing effects at the metal center, i.e. more electron withdrawing on the F-rich and highly steric side. Such F-effects brought about positive influences on the both the catalytic performance of Ni complexes and chain-growth process in ethylene polymerization. It is very interesting to explore the role of such "metal center polarization" in future catalyst designs, which is the "key" to further optimize the catalytic behaviors of such related catalysts. This *N*-aryl moiety with –OH group also enables the capacity to covalently tether theses Ni catalysts on inorganic nanoparticles (SiO_2, Al_2O_3, $MgCl_2$, etc.) for ethylene heterogeneous polymerization.

CRediT authorship contribution statement

Ruikai Wu: Conceptualization, Methodology, Formal analysis, Investigation, Data curation, Writing – original draft. **Lucas Stieglitz:**

Investigation, Writing – review & editing. **Sandro Lehner:** Investigation, Writing – review & editing. **Milijana Jovic:** Investigation, Writing – review & editing. **Daniel Rentsch:** Investigation, Writing – review & editing. **Antonia Neels:** Investigation, Writing – review & editing. **Sabyasachi Gaan:** Project administration, Writing – review & editing, Supervision. **Bernhard Rieger:** Writing – review & editing, Supervision. **Manfred Heuberger:** Project administration, Writing – review & editing, Supervision, Funding acquisition.

Declaration of Competing Interest

The authors declare that they have no known competing financial interests or personal relationships that could have appeared to influence the work reported in this paper.

Data availability

The raw/processed data required to reproduce these findings cannot be shared at this time as the data also forms part of an ongoing study.

Acknowledgement

This work was financially supported by Subitex grant, Switzerland (2020–2025) and China Scholarships Council (No. 201904910562). The NMR hardware was partially granted by the Swiss National Science Foundation (SNSF, Grant 206021_150638/1). The authors are grateful to Feng-Sen Sun (LMU) for his kind help with ESI-HRMS measurements and interpretations.

Appendix A. Supplementary material

Supplementary data to this article can be found online at https://doi.org/10.1016/j.eurpolymj.2023.111830.

References

[1] G. Zanchin, G. Leone, Polyolefin thermoplastic elastomers from polymerization catalysis: advantages, pitfalls and future challenges, Prog. Polym. Sci. 113 (2021), 101342.
[2] C. Chen, Designing catalysts for olefin polymerization and copolymerization: beyond electronic and steric tuning, Nat. Rev. Chem. 2 (5) (2018) 6–14.
[3] H.G. Alt, A. Köppl, Effect of the nature of metallocene complexes of group IV metals on their performance in catalytic ethylene and propylene polymerization, Chem. Rev. 100 (4) (2000) 1205–1222.
[4] G.W. Coates, Precise control of polyolefin stereochemistry using single-site metal catalysts, Chem. Rev. 100 (4) (2000) 1223–1252.
[5] Z. Chen, M. Brookhart, Exploring ethylene/polar vinyl monomer copolymerizations using Ni and Pd α-diimine catalysts, Accounts Chem. Res. 51 (8) (2018) 1831–1839.
[6] A. Nakamura, S. Ito, K. Nozaki, Coordination− insertion copolymerization of fundamental polar monomers, Chem. Rev. 109 (11) (2009) 5215–5244.
[7] A. Nakamura, T.M. Anselment, J. Claverie, B. Goodall, R.F. Jordan, S. Mecking, B. Rieger, A. Sen, P.W. Van Leeuwen, K. Nozaki, Ortho-phosphinobenzenesulfonate: A superb ligand for palladium-catalyzed coordination–insertion copolymerization of polar vinyl monomers, Accounts Chem. Res. 46 (7) (2013) 1438–1449.
[8] C. Tan, C. Chen, Emerging palladium and nickel catalysts for copolymerization of olefins with polar monomers, Angew. Chem. Int. Ed. Engl. 58 (22) (2019) 7192–7200.
[9] H. Mu, G. Zhou, X. Hu, Z. Jian, Recent advances in nickel mediated copolymerization of olefin with polar monomers, Coordin. Chem. Rev. 435 (2021).
[10] Z. Chen, M. Brookhart, exploring ethylene/polar vinyl monomer copolymerizations using Ni and Pd alpha-diimine catalysts, Acc. Chem. Res. 51 (8) (2018) 1831–1839.
[11] F.Z. Wang, C.L. Chen, A continuing legend: the Brookhart-type alpha-diimine nickel and palladium catalysts, Polym. Chem. 10 (19) (2019) 2354–2369.
[12] S.D. Ittel, L.K. Johnson, M. Brookhart, Late-metal catalysts for ethylene homo-and copolymerization, Chem. Rev. 100 (4) (2000) 1169–1204.
[13] S. Dai, C. Chen, A self-supporting strategy for gas-phase and slurry-phase ethylene polymerization using late-transition-metal catalysts, Angew. Chem. Int. Ed. 59 (35) (2020) 14884–14890.
[14] L.K. Johnson, C.M. Killian, M. Brookhart, New Pd (II)-and Ni (II)-based catalysts for polymerization of ethylene and. alpha.-olefins, J. Am. Chem. Soc. 117 (23) (1995) 6414–6415.
[15] L.K. Johnson, S. Mecking, M. Brookhart, Copolymerization of ethylene and propylene with functionalized vinyl monomers by palladium (II) catalysts, J. Am. Chem. Soc. 118 (1) (1996) 267–268.
[16] Z. Guan, P. Cotts, E. McCord, S. McLain, Chain walking: a new strategy to control polymer topology, Science 283 (5410) (1999) 2059–2062.
[17] Z. Wang, Q.B. Liu, G.A. Solan, W.H. Sun, Recent advances in Ni-mediated ethylene chain growth: N-imine-donor ligand effects on catalytic activity, thermal stability and oligo-/polymer structure, Coordin. Chem. Rev. 350 (2017) 68–83.
[18] Q. Mahmood, X. Li, L. Qin, L. Wang, W.-H. Sun, Structural evolution of iminopyridine support for nickel/palladium catalysts in ethylene (oligo) polymerization, Dalton Trans. (Cambridge, England: 2003) (2022).
[19] R. Wu, Y. Wang, R. Zhang, C.-Y. Guo, Z. Flisak, Y. Sun, W.-H. Sun, Finely tuned nickel complexes as highly active catalysts affording branched polyethylene of high molecular weight: 1-(2,6-Dibenzhydryl-4- methoxyphenylimino)-2-(arylimino) acenaphthylenenickel halides, Polymer 153 (2018) 574–586.
[20] R. Wu, W.K. Wu, L. Stieglitz, S. Gaan, B. Rieger, M. Heuberger, Recent advances on α-diimine Ni and Pd complexes for catalyzed ethylene (Co) polymerization: a comprehensive review, Coordin. Chem. Rev. 474 (2023), 214844.
[21] J.L. Rhinehart, L.A. Brown, B.K. Long, A robust Ni (II) α-diimine catalyst for high temperature ethylene polymerization, J. Am. Chem. Soc. 135 (44) (2013) 16316–16319.
[22] J.L. Rhinehart, N.E. Mitchell, B.K. Long, Enhancing α-diimine catalysts for high-temperature ethylene polymerization, ACS Catal. 4 (8) (2014) 2501–2504.
[23] G. Wang, D. Peng, Y. Sun, C. Chen, Interplay of supramolecular chemistry and photochemistry with palladium-catalyzed ethylene polymerization, CCS Chemistry 3 (7) (2021) 2025–2034.
[24] M. Schmid, R. Eberhardt, M. Klinga, M. Leskelä, B. Rieger, New C 2 V-and chiral C 2-symmetric olefin polymerization catalysts based on nickel (II) and palladium (II) diimine complexes bearing 2, 6-diphenyl aniline moieties: synthesis, structural characterization, and first insight into polymerization properties, Organometallics 20 (11) (2001) 2321–2330.
[25] D. Meinhard, M. Wegner, G. Kipiani, A. Hearley, P. Reuter, S. Fischer, O. Marti, B. Rieger, New nickel (II) diimine complexes and the control of polyethylene microstructure by catalyst design, J. Am. Chem. Soc. 129 (29) (2007) 9182–9191.
[26] C.S. Popeney, A.L. Rheingold, Z. Guan, Nickel (II) and palladium (II) polymerization catalysts bearing a fluorinated cyclophane ligand: stabilization of the reactive intermediate, Organometallics 28 (15) (2009) 4452–4463.
[27] Y. Zheng, S. Jiang, M. Liu, Z. Yu, Y. Ma, G.A. Solan, W. Zhang, T. Liang, W.-H. Sun, High molecular weight PE elastomers through 4, 4-difluorobenzhydryl substitution in symmetrical α-diimino-nickel ethylene polymerization catalysts, RSC Adv. 12 (37) (2022) 24037–24049.
[28] D. Peng, C. Chen, Photoresponsive palladium and nickel catalysts for ethylene polymerization and copolymerization, Angew. Chem. Int. Ed. 60 (41) (2021) 22195–22200.
[29] X. Hu, X. Kang, Y. Zhang, Z. Jian, Facile access to polar-functionalized ultrahigh molecular weight polyethylene at ambient conditions, CCS Chem. 4 (5) (2022) 1680–1694.
[30] A. Chen, D. Liao, C. Chen, Promoting Ethylene (co) Polymerization in Aliphatic Hydrocarbon Solvents Using tert-Butyl Substituted Nickel Catalysts, Chin. J. Chem. 40 (2) (2022) 215–222.
[31] Q. Wang, Z. Zhang, C. Zou, C. Chen, A general cocatalyst strategy for performance enhancement in nickel catalyzed ethylene (co) polymerization, Chin. Chem. Lett. 33 (9) (2022) 4363–4366.
[32] W. Yang, M. Meraz, T.T. Fidelis, W.H. Sun, The quantitative influence of coordinated halogen atoms on the catalytic performance of bisiminoacenaphthylnickel complexes in ethylene polymerization, ChemPhysChem 22 (6) (2021) 585–592.
[33] M. Liu, R. Zhang, Y. Ma, M. Han, G.A. Solan, W. Yang, T. Liang, W.-H. Sun, Trifluoromethoxy-substituted nickel catalysts for producing highly branched polyethylenes: impact of solvent, activator and N, N′-ligand on polymer properties, Polym. Chem. 13 (8) (2022) 1040–1058.
[34] G. Zohuri, S. Damavandi, R. Sandaroos, S. Ahmadjo, Ethylene polymerization using fluorinated FI Zr-based catalyst, Polym. Bull. 66 (8) (2011) 1051–1062.
[35] M. Qasim, M.S. Bashir, S. Iqbal, Q. Mahmood, Recent advancements in α-diimine-nickel and -palladium catalysts for ethylene polymerization, Eur. Polym. J. 160 (2021), 110783.
[36] M. Schnitte, S. Lipinski, E. Schiebel, S. Mecking, Pentafluorophenyl groups as remote substituents in Ni (II) polymerization catalysis, Organometallics 39 (1) (2019) 13–17.
[37] M. Schnitte, J.S. Scholliers, K. Riedmiller, S. Mecking, Remote perfluoroalkyl substituents are key to living aqueous ethylene polymerization, Angew. Chem. Int. Ed. 59 (8) (2020) 3258–3263.
[38] Y. Wang, R. Gao, Q. Gou, J. Lai, R. Zhang, X. Li, Z. Guo, Developments in late transition metal catalysts with high thermal stability for ethylene polymerization: a crucial aspect from laboratory to industrialization, Eur. Polym. J. (2022), 111693.
[39] S. Ahmadjo, S. Damavandi, G. Zohuri, A. Farhadipour, Z. Etemadinia, Mechanisms for the effects of fluorine and α-diimine backbone structure on the catalyst behavior and catalyst deactivation in ethylene polymerization by Ni catalysts, J. Organomet. Chem. 835 (2017) 43–51.
[40] S. Liao, X.-L. Sun, Y. Tang, Side arm strategy for catalyst design: modifying bisoxazolines for remote control of enantioselection and related, Accounts Chem. Res. 47 (8) (2014) 2260–2272.
[41] J. Wang, L. Wang, H. Yu, R.S. Ullah, M. Haroon, A. Zain ul, X. Xia, R.U. Khan, Recent progress in ethylene polymerization catalyzed by Ni and Pd catalysts, Eur. J. Inorg. Chem. 2018 (13) (2018) 1450–1468.

[42] Q. Muhammad, C. Tan, C. Chen, Concerted steric and electronic effects on α-diimine nickel-and palladium-catalyzed ethylene polymerization and copolymerization, Sci. Bull. 65 (4) (2020) 300–307.
[43] X. Hu, X. Kang, Z. Jian, Suppression of chain transfer at high temperature in catalytic olefin polymerization, Angew. Chem. Int. Ed. 61 (33) (2022) e202207363.
[44] C. Tan, C. Zou, C. Chen, An ionic cluster strategy for performance improvements and product morphology control in metal-catalyzed olefin–polar monomer copolymerization, J. Am. Chem. Soc. 144 (5) (2022) 2245–2254.
[45] F. Wang, C. Chen, A continuing legend: the Brookhart-type α-diimine nickel and palladium catalysts, Polym. Chem. 10 (19) (2019) 2354–2369.
[46] L. Guo, S. Dai, C. Chen, Investigations of the ligand electronic effects on α-diimine nickel (II) catalyzed ethylene polymerization, Polymers 8 (2) (2016) 37.
[47] H. Liu, W. Zhao, X. Hao, C. Redshaw, W. Huang, W.-H. Sun, 2, 6-Dibenzhydryl-N-(2-phenyliminoacenaphthylenylidene)-4-methylbenzenamine nickel dibromides: synthesis, characterization, and ethylene polymerization, Organometallics 30 (8) (2011) 2418–2424.
[48] Z. Wang, Q. Liu, G.A. Solan, W.-H. Sun, Recent advances in Ni-mediated ethylene chain growth: Nimine-donor ligand effects on catalytic activity, thermal stability and oligo-/polymer structure, Coordin. Chem. Rev. 350 (2017) 68–83.
[49] F. Zhai, J.B. Solomon, R.F. Jordan, Copolymerization of ethylene with acrylate monomers by amide-functionalized α-diimine Pd catalysts, Organometallics 36 (9) (2017) 1873–1879.
[50] O.V. Dolomanov, L.J. Bourhis, R.J. Gildea, J.A. Howard, H. Puschmann, OLEX2: a complete structure solution, refinement and analysis program, J. Appl. Cryst. 42 (2) (2009) 339–341.
[51] M.C. Burla, R. Caliandro, M. Camalli, B. Carrozzini, G.L. Cascarano, L. De Caro, C. Giacovazzo, G. Polidori, D. Siliqi, R. Spagna, IL MILIONE: a suite of computer programs for crystal structure solution of proteins, J. Appl. Cryst. 40 (3) (2007) 609–613.
[52] G.M. Sheldrick, SHELXT–Integrated space-group and crystal-structure determination, Acta Crystall. Sect.: Found. Adv. 71 (1) (2015) 3–8.
[53] R. Wu, Y. Wang, L. Guo, C.Y. Guo, T. Liang, W.H. Sun, Highly branched and high-molecular-weight polyethylenes produced by 1-[2,6-bis(bis(4-fluorophenyl) methyl)-4-MeOC6H2N]-2-aryliminoacenaphthylnickel(II) halides, J. Polym. Sci. A Polym. Chem. 57 (2) (2018) 130–145.
[54] Y. Yan, S.-F. Yuan, M. Liu, G.A. Solan, Y.-P. Ma, T.-L. Liang, W.-H. Sun, Investigating the effects of para-methoxy substitution in sterically enhanced unsymmetrical bis (arylimino) pyridine-cobalt ethylene polymerization catalysts, Chin. J. Polym. Sci. 40 (3) (2022) 266–279.
[55] S. Dai, X. Sui, C. Chen, Highly robust palladium (II) α-diimine catalysts for slow-chain-walking polymerization of ethylene and copolymerization with methyl acrylate, Angew. Chem. 127 (34) (2015) 10086–10091.
[56] X. Wang, L. Fan, Y. Ma, C.-Y. Guo, G.A. Solan, Y. Sun, W.-H. Sun, Elastomeric polyethylenes accessible via ethylene homo-polymerization using an unsymmetrical α-diimino-nickel catalyst, Polym. Chem. 8 (18) (2017) 2785–2795.
[57] Q. Mahmood, Y. Zeng, E. Yue, G.A. Solan, T. Liang, W.-H. Sun, Ultra-high molecular weight elastomeric polyethylene using an electronically and sterically enhanced nickel catalyst, Polym. Chem. 8 (41) (2017) 6416–6430.
[58] D.H. Camacho, Z.B. Guan, Designing late-transition metal catalysts for olefin insertion polymerization and copolymerization, Chem. Commun. 46 (42) (2010) 7879–7893.
[59] J.R. Severn, J.C. Chadwick, R. Duchateau, N. Friederichs, "Bound but not gagged" immobilizing single-site α-olefin polymerization catalysts, Chem. Rev. 105 (11) (2005) 4073–4147.
[60] M.M. Stalzer, M. Delferro, T.J. Marks, Supported single-site organometallic catalysts for the synthesis of high-performance polyolefins, Catal. Lett. 145 (1) (2014) 3–14.
[61] I.E. Soshnikov, N.V. Semikolenova, K.P. Bryliakov, A.A. Antonov, W.-H. Sun, E. P. Talsi, Nature of heterobinuclear Ni (I) complexes formed upon the activation of the α-diimine complex LNiIIBr 2 with AlMe3 and MMAO, Organometallics 40 (7) (2021) 907–914.
[62] C. Tan, W.-M. Pang, C.-L. Chen, A phenol-containing α-diimine ligand for nickel- and palladium-catalyzed ethylene polymerization, Chin. J. Polym. Sci. 37 (10) (2019) 974–980.
[63] Y. Zhang, C. Wang, S. Mecking, Z. Jian, Ultrahigh branching of main-chain-functionalized polyethylenes by inverted insertion selectivity, Angew. Chem. Int. Ed. Engl. 59 (34) (2020) 14296–14302.
[64] X. Wang, L. Fan, Y. Yuan, S. Du, Y. Sun, G.A. Solan, C.-Y. Guo, W.-H. Sun, Raising the N-aryl fluoride content in unsymmetrical diaryliminoacenaphthylenes as a route to highly active nickel (II) catalysts in ethylene polymerization, Dalton Trans. 45 (45) (2016) 18313–18323.
[65] S. Du, S. Kong, Q. Shi, J. Mao, C. Guo, J. Yi, T. Liang, W.-H. Sun, Enhancing the activity and thermal stability of nickel complex precatalysts using 1-[2, 6-bis (bis (4-fluorophenyl) methyl)-4-methyl phenylimino]-2-aryliminoacenaphthylene derivatives, Organometallics 34 (3) (2015) 582–590.
[66] Y. Wang, A. Vignesh, M. Qu, Z. Wang, Y. Sun, W.-H. Sun, Access to polyethylene elastomers via ethylene homo-polymerization using N, N′-nickel (II) catalysts appended with electron withdrawing difluorobenzhydryl group, Eur. Polym. J. 117 (2019) 254–271.
[67] Q. Zhang, R. Zhang, Y. Ma, G.A. Solan, T. Liang, W.-H. Sun, Branched polyethylenes attainable using thermally enhanced bis (imino) acenaphthene-nickel catalysts: Exploring the effects of temperature and pressure, Appl. Catal. A 573 (2019) 73–86.
[68] R. Zhang, Z. Wang, Y. Ma, G.A. Solan, Y. Sun, W.-H. Sun, Plastomeric-like polyethylenes achievable using thermally robust N, N′-nickel catalysts appended with electron withdrawing difluorobenzhydryl and nitro groups, Dalton Trans. 48 (5) (2019) 1878–1891.
[69] Q. Liu, W. Zhang, D. Jia, X. Hao, C. Redshaw, W.-H. Sun, 2-{2, 6-Bis [bis (4-fluorophenyl) methyl]-4-chlorophenylimino}-3-aryliminobutylnickel (II) bromide complexes: synthesis, characterization, and investigation of their catalytic behavior, Appl. Catal. A 475 (2014) 195–202.
[70] M. Khoshsefat, Y. Ma, W.-H. Sun, Multinuclear late transition metal catalysts for olefin polymerization, Coordin. Chem. Rev. 434 (2021).
[71] F.-S. Liu, H.-B. Hu, Y. Xu, L.-H. Guo, S.-B. Zai, K.-M. Song, H.-Y. Gao, L. Zhang, F.-M. Zhu, Q. Wu, Thermostable α-diimine nickel (II) catalyst for ethylene polymerization: effects of the substituted backbone structure on catalytic properties and branching structure of polyethylene, Macromolecules 42 (20) (2009) 7789–7796.
[72] S. Dai, S. Li, G. Xu, C. Chen, Direct synthesis of polar functionalized polyethylene thermoplastic elastomer, Macromolecules 53 (7) (2020) 2539–2546.
[73] K. Patel, S.H. Chikkali, S. Sivaram, Ultrahigh molecular weight polyethylene: catalysis, structure, properties, processing and applications, Prog. Polym. Sci. 109 (2020).
[74] G.B. Galland, R.F. de Souza, R.S. Mauler, F.F. Nunes, 13C NMR determination of the composition of linear low-density polyethylene obtained with [η3-methallyl-nickel-diimine] PF6 complex, Macromolecules 32 (5) (1999) 1620–1625.
[75] L. Stieglitz, D. Henschel, T. Pehl, B. Rieger, In situ activation: chances and limitations to form ultrahigh molecular weight syndiotactic polypropylene with metallocene dichlorides, Organometallics 40 (24) (2021) 4055–4065.